N-Nervonoylsphingomyelin (C24:1) Prevents Lateral Heterogeneity in Cholesterol-Containing Membranes

Sabina Maté,[†*] Jon V. Busto,[‡] Aritz B. García-Arribas,[‡] Jesús Sot,[‡] Romina Vazquez,[†] Vanesa Herlax,[†] Claude Wolf,[§] Laura Bakás,[¶] and Félix M. Goñi[‡]

[†]Instituto de Investigaciones Bioquímicas de La Plata (INIBIOLP), Centro Cientifico Tecnológico La Plata, Consejo Nacional de Investigaciones Científicas y Tecnicas, Facultad de Ciencias Médicas, Universidad Nacional de La Plata, La Plata, Argentina; [‡]Unidad de Biofísica-Centro Mixto, Consejo Superior de Investigaciones Científicas, Universidad del País Vasco/Euskal Herriko Unibertsitatea, Bilbao, Spain; [§]Groupe de spectrométrie de masse-APLIPID, Université Pierre et Marie Curie, Faculté de Médicine Pierre et Marie Curie, Paris, France; and [¶]Departamento de Ciencias Biológicas. Facultad de Ciencias Exactas. Universidad Nacional de La Plata, La Plata, Argentina

ABSTRACT This study was conducted to explore how the nature of the acyl chains of sphingomyelin (SM) influence its lateral distribution in the ternary lipid mixture SM/cholesterol/1,2-dioleoyl-*sn*-glycero-3-phosphocholine (DOPC), focusing on the importance of the hydrophobic part of the SM molecule for domain formation. Atomic force microscopy (AFM) measurements showed that the presence of a double bond in the 24:1 SM molecule in mixtures with cholesterol (CHO) or in pure bilayers led to a decrease in the molecular packing. Confocal microscopy and AFM showed, at the meso- and nanoscales respectively, that unlike 16:0 and 24:0 SM, 24:1 SM does not induce phase segregation in ternary lipid mixtures with DOPC and CHO. This ternary lipid mixture had a nanomechanical stability intermediate between those displayed by liquid-ordered (Lo) and liquid-disordered (Ld) phases, as reported by AFM force spectroscopy measurements, demonstrating that 24:1 SM is able to accommodate both DOPC and CHO, forming a single phase. Confocal experiments on giant unilamellar vesicles made of human, sheep, and rabbit erythrocyte ghosts rich in 24:1 SM and CHO, showed no lateral domain segregation. This study provides insights into how the specific molecular structure of SM affects the lateral behavior and the physical properties of both model and natural membranes. Specifically, the data suggest that unsaturated SM may help to keep membrane lipids in a homogeneous mixture rather than in separate domains.

INTRODUCTION

Sphingomyelins (SMs) and phosphatidylcholines (PCs) are major lipid classes in the mammalian cell plasma-membrane outer leaflet. Naturally occurring SMs have a phosphocholine headgroup esterified to the C1 hydroxyl group of a long-chain sphingoid base. The most common long-chain base in mammalian SM is sphingosine (1). Typically, the acyl chains amide-linked to carbon 2 of the sphingoid base are long (16–24 carbon atoms) and saturated, but 24:1 has also been recognized recently as a common N-linked acyl chain in natural SMs (2,3).

A preferential interaction between SM and cholesterol (CHO) in both cell and model membranes has been proposed as a key factor in the formation of CHO- and SM-rich domains in membranes (4–6). CHO and SM have both hydrogen-bond donor and acceptor groups that together with the CHO flat and extended hydrophobic structure promote the tight packing of SM and CHO into the liquid-ordered (Lo) arrangement (7). Lo-state bilayers form when CHO is mixed with a lipid with a high gel/fluid melting temperature (e.g., SM). The Lo phase is an intermediate physical state that exhibits a tight lipid packing, similar to the gel phase but with high lipid lateral diffusion rates, only slightly smaller than those of the fluid or liquid-disordered (Ld) phase (8). Many authors refer to the presence of Lo domains enriched in SM and CHO in biological membranes. However some confusion exists regarding the definition of lateral phases and the distinction between the concepts of rafts, Lo domains, and detergent-resistant membranes, as highlighted by Lichtenberg et al. (9). Despite the importance of Lo domains, the role of SM molecular diversity in their formation and biological significance is not completely understood. In this context, the effect of various structural features of SM on its interaction with CHO for domain stabilization has been investigated by Slotte and co-workers (10–13). Those authors have shown that modifications of the SM molecule headgroup (10) or long-chain base (11,12), as well as changes in the stereoconfiguration (13), influence domain stabilization.

24:1 SM is now known to be present in mammalian plasma membranes, but its influence on the physical properties of the bilayer has not been explored. Both 24:0 SM and 24:1 SM have been examined by Jimenez-Rojo et al. (14) from the point of view of their thermotropic phase behavior. Both lipids exhibit complex endotherms for the gel-fluid transition, suggesting the formation of partially interdigitated domains. The unsaturated C24:1 SM melts at ~20°C lower than its saturated counterpart. This study is intended to investigate the relevance of the SM hydrophobic moiety in the lateral separation of membrane domains, by comparing 24:1 SM, 24:0 SM, and 16:0 SM. Confocal

Submitted March 13, 2014, and accepted for publication April 23, 2014.

*Correspondence: smate@med.unlp.edu.ar

Editor: Simon Scheuring.

0006-3495/14/06/2606/11 $2.00

http://dx.doi.org/10.1016/j.bpj.2014.04.054

microscopy and atomic force microscopy (AFM) were used for imaging, at meso and nanoscale, respectively, the lateral phase behavior of ternary lipid mixtures composed of DOPC, SM, and CHO. Mechanical stability of supported bilayers made of pure SM, SM/CHO, and DOPC/SM/CHO mixtures was studied by AFM force spectroscopy measurements. Finally, we performed fluorescence confocal microscopy observations on human, sheep, and rabbit erythrocyte membranes, which have a wide structural diversity in the SM acyl chains. The various data show a clear effect of 24:1 SM in suppressing SM/CHO domain segregation in both model and biological membranes while keeping a high degree of lipid order. This suggests that unsaturation in SM may constitute an important mechanism to ensure lipid mixing in cell membranes, even in the presence of CHO.

MATERIALS AND METHODS

Reagents

Sheep and rabbit blood were kindly provided by Facultad de Ciencias Veterinarias of the Universidad Nacional de La Plata. Human blood was obtained from a subject who gave the appropriate informed consent. Cells were washed with saline (9 g/L NaCl) and stored in Alsever solution from Sigma-Aldrich (St. Louis, MO). 1,2-dioleoyl-*sn*-glycero-3-phosphocholine (DOPC), N-palmitoyl-D-erythro-sphingosylphosphorylcholine (16:0 SM), N-lignoceroyl-D-erythro-sphingosylphosphorylcholine (24:0 SM) and N-nervonoyl-D-erythro-sphingosylphosphorylcholine (24:1 SM) were purchased from Avanti Polar Lipids (Birmingham, AL). Cholesterol, naphtho [2,3a-]pyrene and lipid standards for mass spectrometric determinations were obtained from Sigma-Aldrich. N-(Lissamine Rhodamine B sulfonyl) dioleoylphosphatidylethanolamine (Liss-Rho-DOPE) was purchased from Avanti Polar Lipids.

Ethics statement

Blood from healthy sheep and rabbit was obtained following a protocol approved by the Research Ethics Committee of the Facultad de Ciencias Veterinarias of the Universidad Nacional de La Plata (CICUAL 129/09) in accordance with international guidelines for the care and use of laboratory animals. All the studies performed with erythrocytes were approved by the Institutional Review Board of the INIBIOLP and were carried out in accordance with the Guide for the Care and Use of Laboratory Animals (Instituto de Investigaciones Bioquimicas de La Plata, Animal Welfare Assurance No. A5647-01).

Confocal microscopy measurements

Sample preparation

Preparation of G-ghosts from erythrocyte membranes. Human, sheep, and rabbit erythrocytes were isolated from fresh blood and washed three times (or until supernatant was clear) with 25 mM HEPES, 150 mM NaCl, pH 7.4 (assay buffer), by centrifugation at 1250 $\times$ *g* for 10 min at 4°C. The supernatant was discarded and the erythrocyte-containing pellet was used for forming ghosts. Right-side-out ghosts and giant vesicles from erythrocyte membranes (G-ghosts) were prepared as described in Montes et al. (15).

Electroformation of giant unilamellar vesicles. Giant unilamellar vesicles (G-ghosts and GUVs) were prepared by electroformation on a pair of platinum (Pt) wires by a method first developed by Angelova and Dimitrov (16), (17), modified as described previously (15). Lipid stock solutions were prepared in 2:1 (v/v) chloroform/methanol at 0.27 mg/mL, and appropriate volumes of each preparation were mixed. Labeling was carried out by premixing the desired fluorescent probes with the lipids in organic solvent. We have used N-(Lissamine Rhodamine B sulfonyl) dioleoylphosphatidylethanolamine (Liss-Rho-DOPE) as a marker for Ld phases and naphtho [2,3a-]pyrene (NAP) for Lo phases. The average concentration of individual fluorescent probes in each sample was 0.2 mol %. The fluorescent probes, in 2 μL lipid mixtures, were deposited on platinum (Pt) wires. The Pt wires were placed under vacuum for 2 h to completely remove the organic solvent. The sample was covered to avoid light exposure and allowed to precipitate onto the Pt wires for 5 min.

One side of the chamber was then sealed with a coverslip. We added 500 μL assay buffer, prepared with high-purity water (SuperQ, Millipore, Billerica, MA) heated at 60°C, until it covered the Pt wires and the latter were connected to a TG330 function generator (Thurlby Thandar Instruments, Huntingdon, UK). The alternating current field was applied in three steps, all performed at 60°C: 1), frequency 500 Hz, amplitude 220 mV (35 V/m) for 5 min; 2), frequency 500 Hz, amplitude 1900 mV (313 V/m) for 20 min; and 3), frequency 500 Hz, amplitude 5.3 V (870 V/m) for 90 min. The temperatures used for GUV formation correspond to those at which the different membranes display a single fluid phase.

Microscopy

GUVs were imaged with confocal microscopy using a Nikon D-eclipse C1 confocal system (Nikon, Tokyo, Japan). The excitation wavelengths used for excitation were 458 nm for NAP and 561 nm for Liss-Rho-DOPE. Fluorescence emission was retrieved at 465–505 nm for NAP and at 573–613 nm for Liss-Rho-PE.

AFM measurements

Multilamellar vesicle preparation

Multilamellar vesicles (MLVs) were prepared by mixing the appropriate amounts of synthetic pure lipids (16:0 SM; 24:0 SM; and 24:1 SM, DOPC, CHO) dissolved in chloroform/methanol (2:1, v/v). The samples were dried by evaporating the solvent under a stream of nitrogen and kept under high vacuum for 2 h. The samples were hydrated in 25 mM Hepes, 150 mM NaCl, and 3 mM $CaCl_2$, pH 7.4 (assay buffer containing $CaCl_2$), prepared with high-purity water (Millipore SuperQ), with dispersion aided by stirring. Final lipid concentration was 0.5 mM.

Supported planar bilayer preparation

Planar bilayer preparation on mica substrates for AFM measurements was performed using a vesicle adsorption technique (18). MLVs were prepared as described previously. After completing lipid detachment from the bottom of the test tube, MLVs were introduced in a FB-15049 (Fisher Scientific, Waltham, MA) bath sonicator and kept at 65°C for 1 h. In this way, small unilamellar vesicles (SUVs) were generated. Thereafter, 120 μL assay buffer containing $CaCl_2$ was added onto a 1.2 cm^2 freshly cleaved mica substrate previously mounted onto a BioCell cover slip-based liquid cell for AFM measurements (JPK Instruments, Berlin, Germany). Sonicated vesicles (60 μL) were then added on top of the mica. Final lipid concentration was 150 μM. Vesicles were left to adsorb and extend for 30 min with the sample temperature maintained at 65°C. The samples were left for a further 30 min to equilibrate at room temperature, after which the nonadsorbed vesicles were discarded by washing 10 times with assay buffer in the absence of $CaCl_2$. A small amount of buffer was always left on top of the substrate to maintain hydration of the supported planar bilayers (SPBs) at all times. The Biocell was set to 20°C and the planar bilayers were left to equilibrate for another 30 min before measurements.

AFM imaging

The measurements were performed on a NanoWizard II AFM (JPK Instruments) at a controlled temperature of 22°C. MLCT silicon nitride

cantilevers (Veeco Instruments, Plainview, NY) with a spring constant of 0.1 and/or 0.5 N/m were used in contact-mode scanning (constant vertical deflection) maintaining the minimum possible force. Images were collected at 512 × 512-pixel resolution at a scanning rate between 1 and 1.5 Hz and line-fitted using the JPK Image Processing software as required.

Force spectroscopy measurements

Indentation experiments on supported lipid bilayers were performed as described by Garcia-Manyes et al. (19). Silicon nitride MLCT cantilevers were calibrated in lipid-free solid substrates before contact-mode AFM imaging. The spring constant was independently determined for each of the cantilevers using the thermal noise method. SPBs were then imaged to check for correct extension and for possible lateral segregation. Finally, force spectroscopy curves were performed on the bilayers at 1 μm/s. Breakthrough forces were manually determined for each of the force versus piezo displacement curves as a 4- to 6-nm jump in the extended trace. The resulting histograms were generated from at least three independent sample preparations with at least three different cantilevers (mean ± SD; n = 2500–3700).

Lipid analysis

Determination of cholesterol/phospholipid ratio

Total CHO and phospholipids from erythrocyte ghosts were quantified by an enzymatic assay (Colestat, Wiener Lab, Rosario, Argentina) and a phosphorus colorimetric assay (20), respectively.

Major lipid classes

Total lipids of erythrocyte ghosts were extracted according to the method of Bligh and Dyer (21). Lipids recovered from the chloroform layer were subjected to thin-layer chromatography (TLC) on high-performance TLC plates (Whatman, GE Healthcare, Fairfield, CT) developed subsequently by a two-solvent system, chloroform/methanol/acetic acid/water (25:18.75:1.75:1 by vol), followed by hexane/diethyl ether/acetic acid (40:10:1 v/v). Lipid spots were detected by spraying 5% sulfuric acid in ethanol; then, HPTLC plates were heated at 120°C. Spots were identified by comparison with commercial standards, and quantitation was performed by densitometry using a 1D Image Analysis Software.

Mass spectrometric analysis of SM species from erythrocytes

Lipid extracts prepared from erythrocyte ghosts were analyzed by flow injection liquid chromatography (Agilent 1200, Agilent Technologies, Massy, France) coupled to electrospray ionization-tandem mass spectrometry (ESI-MS/MS) (TQ, API3000, Applied Biosystems-Sciex, Toronto, Canada) as described by Quinn et al. (22). A precursor positive ion scanning of the fragment ion m/z +184 specific for phosphocholine-containing lipids was used for the specific assay of molecular species of PC and SM. Calibrations of the different classes with external standards (Sigma Aldrich) were generated assuming only a small difference in the MS2 response to the variety of biological molecular species. Correction of isotopic overlap of lipid species and peak assignment were performed with the software LIMSA (kindly provided by Dr P. Haïmi, Helsinki University, Helsinki, Finland) using a lipid structure library prepared for human, rodent, and ruminant erythrocyte membranes (22,23).

LUV preparation

For liposome preparation, phospholipids were dissolved in chloroform: methanol (2:1, v/v), and the mixture was evaporated to dryness under a stream of nitrogen. Traces of solvent were removed by evacuating the samples under high vacuum for at least 2 h. The samples were hydrated at 50°C in a buffer of 25 mM HEPES and 150 mM NaCl, pH 7.4. The solution was frozen in liquid nitrogen and thawed at 50°C 10 times. Large unilamellar vesicles (LUVs) were prepared by the extrusion method, using polycarbonate filters with a pore size of 0.1 μm (Nuclepore, Pleasanton, CA). Vesicle sizes were determined by dynamic light scattering using a Zetasizer instrument (Malvern, United Kingdom). The average vesicle diameter was 90–100 nm. The final lipid concentration was measured in terms of lipid phosphorus.

Fluorescence spectroscopy

The generalized polarization (GP) of laurdan was measured in an Aminco Bowman Series 2 spectrofluorometer (ThermoFisher Scientific, Waltham, MA) equipped with thermoregulated cell holders. The excitation GP_{EX} parameter was calculated according to

$$GP_{EX} = (I_{440} - I_{490})/(I_{440} + I_{490})$$

where I_{440} and I_{490} are the emission intensities at 440 and 490 nm, respectively, when exciting at 360 nm. The final probe/lipid molar ratio was 1/1000.

RESULTS

Nanomechanical properties of 24:1 SM-containing bilayers

To study the effect of unsaturation in the 24:1 SM molecule on bilayer packing properties at the meso- and nanoscales, measurements were taken of the mechanical stability of SPBs. SPBs containing 24:1 SM, either pure or in mixtures with CHO, were studied and compared with bilayers containing 24:0 SM or 16:0 SM, the latter being the dominant SM species in most mammalian cells. Preliminary experiments with the samples described in Table 1 had shown that the topography of these bilayers did not reveal any lateral separation of domains (Fig. S1 in the Supporting Material). The topography of SPBs containing 16:0 SM has been discussed extensively in the literature and is not shown here. AFM force spectroscopy measurements provided force curves at a constant piezoelectric velocity of 1 μm s^{-1}. The breakthrough force (F_b) is a property that is strongly dependent on the bilayer chemical composition and represents the maximum force that a bilayer can withstand before rupturing. F_b is used as a measure of the bilayer mechanical stability (19).

TABLE 1 AFM force spectroscopy measurements

Lipid composition of SLBs	F_b
16:0 SM	36.8 ± 3.7 nN (888)
24:0 SM	32.0 ± 5.9 nN (933)
24:1 SM	30.6 ± 2.9 nN (651)
16:0 SM/CHO (7:3 molar ratio)	23.7 ± 2.0 nN (875)
24:1 SM/CHO (7:3 molar ratio)	17.9 ± 1.6 nN (786)

Average breakthrough forces, F_b, were from indentation measurements on SLBs made of 16:0 SM and 24:1 SM, either pure or mixed with CHO. Values are represented as the mean ± SD. The number of measurements for each value is indicated in parentheses. Differences were statistically significant; Student's t-test, $p < 0.0001$.

Fig. 1 depicts the experiments corresponding to 24:1 SM and 24:0 SM SPBs. Table 1 shows the average rupture force for SPBs made of various pure SMs and of SM/CHO binary mixtures. Data for the pure SMs show a relatively small effect of chain length or unsaturation on the measured F_b. For the mixtures of 16:0 SM/CHO and 24:1 SM/CHO the average indentation forces measured were 23.7 nN and 17.9 nN, respectively, showing that CHO causes a decrease in the bilayer breakthrough force. It is interesting in this context that 16:0 SM will be in the gel phase at the temperature of the measurements (~22°C), whereas according to published phase diagrams, addition of 30 mol % CHO may lead to a situation of gel-Lo coexistence. The available F_b data are, however, insufficient to interpret the difference in F_b in terms of phase structure; thus, we are limited to stating the effect of CHO lowering F_b for both 16:0 SM and 24:1 SM bilayers. In both cases, CHO decreases F_b by the same amount, ~13 nN.

As for the morphology of the force curves of 24:1 SM and 24:0 SM SPBs, differences can be observed in the approaching regions of the curves. When the tip reaches the bilayer consisting of 24:1 SM (Fig. 1 *A*), a gradual increase in slope is observed, whereas for 24:0 SM bilayers (Fig. 1 *B*), the change in slope is abrupt. In addition, the breakthrough event is far clearer for 24:1 SM than for 24:0 SM (see inset). A condition that could explain the observed slope at the moment of tip-SPB contact could be the jump-to-contact phenomenon, which would occur when attractive forces exceed both the cantilever spring constant and the repulsive forces (24). Since this is not frequently observed in liquid experiments (also depending on ionic strength) (25), we consider that jump-to-contact is not at the origin of this effect. Moreover, jump-to-contact can cause negative force detection in the approaching curves (26), and no such forces are detected in our study. We suggest that this effect is caused by the difference in degree of viscoelasticity of the SPBs, which would explain as well the differences in the morphology of the breakthrough event.

Confocal microscopy and lateral organization of ternary DOPC/SM/CHO mixtures

PC/SM/CHO ternary mixtures are commonly used to study the physical properties of membranes exhibiting Lo-Ld domain coexistence. Confocal microscopy experiments were performed to study the effect of SM unsaturation on its interaction with DOPC or CHO and on domain formation. 16:0 SM, 24:1 SM, and 24:0 SM were used to discriminate the influence of unsaturation and length of the N-amide-linked acyl chain on SM phase behavior. The identification of lipid membrane heterogeneity by fluorescence microscopy relies on membrane markers with well-defined partitioning behavior. We used Liss-Rho-DOPE as a marker for Ld phases (27) and NAP for Lo phases. The NAP partitioning behavior indicates that hydrophobic, disk-shaped molecules partition preferentially into the Lo phase. The relatively high photostability of NAP makes it suitable for studying the properties of Lo phases by fluorescence methods (28,29).

Fig. 2 shows GUVs labeled with Liss-Rho-DOPE and NAP and imaged at 20°C. GUVs made of DOPC/16:0 SM/CHO and DOPC/24:0 SM/CHO (2:1:1 molar ratio) show heterogeneous distribution of the probes, indicating lateral segregation of phases (Lo and Ld phases), but in GUVs prepared with DOPC/24:1 SM/ CHO, probe

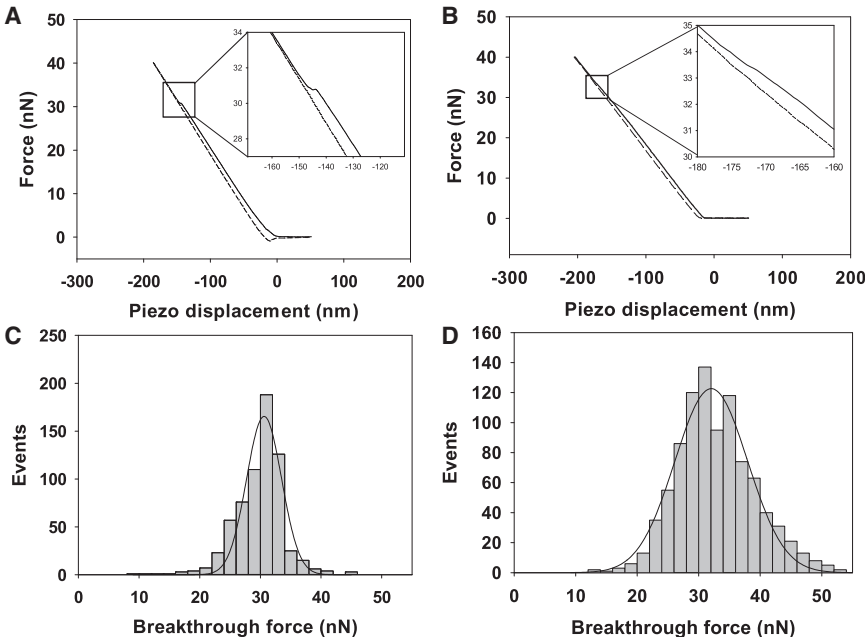

FIGURE 1 Nanomechanical properties of 24:1 SM and 24:0 SM SPBs. (*A* and *B*) Representative force curves on 24:1 SM (*A*) and 24:0 SM (*B*) SPBs. (*C* and *D*) Distribution of force breakthrough events in 24:1 SM (*C*) and 24:0 SM (*D*) SPBs. Solid lines represent Gaussian fittings. Each histogram is based on two samples analyzed with three different tips.

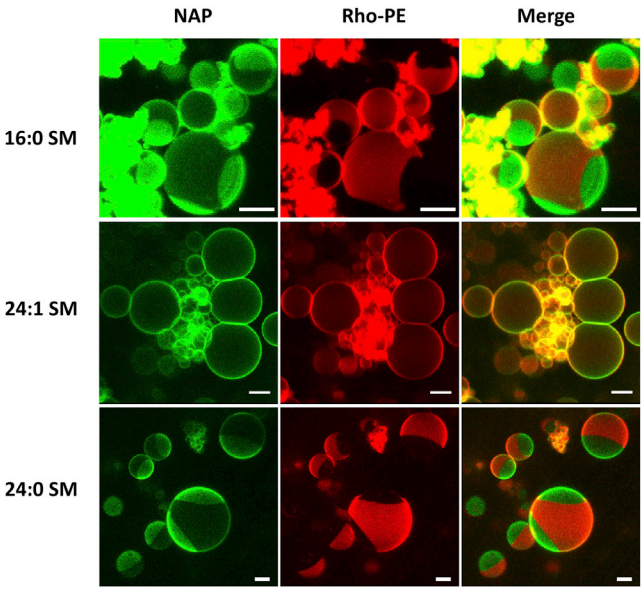

FIGURE 2 Confocal fluorescence microcopy images of Liss-Rho-DOPE- (*red*) and NAP-labeled (*green*) GUVs. Vesicle lipid composition was DOPC/SM/CHO (2:1:1, molar ratio), where the SM acyl chain was 16:0, 24:1, or 24:0. Scale bar, 10 μm.

distribution was homogeneous. These results show that in these systems, unsaturation is more important than acyl chain length for SM phase behavior.

To investigate how the proportions of the different lipids influence the lateral organization of DOPC/16:0 SM/CHO bilayers, GUVs were prepared with 50, 33, and 20 mol %, respectively, of DOPC while keeping 16:0 SM and CHO at a constant 1:1 ratio. Fig. 3 shows that the Ld phase fraction (Rho-PE-stained) decreases with decreasing DOPC concentration, although phase separation occurs even when the DOPC content is as low as 20 mol %.

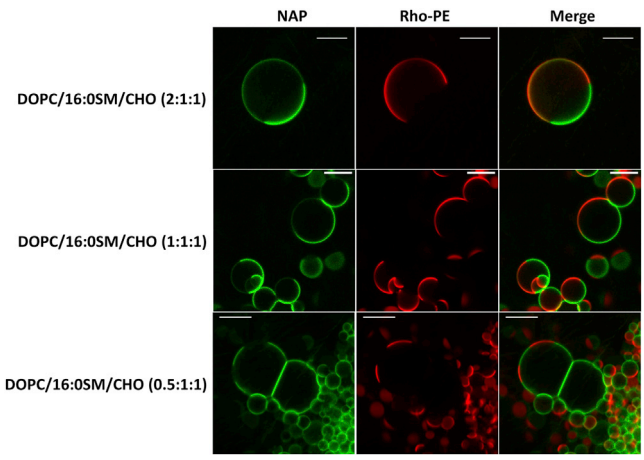

FIGURE 3 Confocal fluorescence microscopy images of Liss-Rho-DOPE- (*red*) and NAP-labeled (*green*) GUVs containing different amounts of DOPC. The lipid composition of the vesicles was DOPC/16:0 SM/CHO (2:1:1, 1:1:1, and 0.5:1:1 molar ratios). Scale bar, 10 μm.

We next studied the effect of the 24:1 SM molar ratio on the lateral organization of these ternary lipid mixtures. Fig. 4 shows probe distribution in GUVs made of DOPC/SM/CHO in 2:1:1, 1:1:1, and 0.5:1:1 molar ratios. For each ternary lipid mixture, different ratios of 24:1 and 16:0 SM were assayed. When both SMs are present, irrespective of the molar ratio tested, the GUVs show a homogeneous distribution of the probe, indicating the existence of a single phase. In summary, confocal microscopy describes a clear effect of 24:1 SM in suppressing SM/CHO domain segregation in ternary mixtures with DOPC. Moreover, 24:1 SM, even at relatively low concentrations (12.5 mol %), prevents phase segregation induced by the presence of 16:0 SM in these ternary lipid mixtures.

Atomic force microscopy of ternary DOPC/SM/CHO mixtures

AFM allows the study of lipid bilayer surface topology in aqueous environments, providing nanometer lateral resolution and Ångström resolution vertically, and allowing visualization of phase-separated lipid domains in planar membranes (30). Fig. 5 *A* illustrates the topography of SPBs prepared with DOPC/16:0 SM/CHO (2:1:1 molar ratio) and imaged in buffer. This image shows coexistence of bright domains with an SM/CHO-enriched Lo structure protruding from the darker-fluid DOPC-enriched matrix, the apparent height difference being 0.6–0.7 nm (see line profile in Fig. 5 *B*). Very similar separation of Ld and Lo phases is seen for the DOPC/24:0 SM/CHO mixture (Fig. 5, *C* and *D*). In line with the GUV results

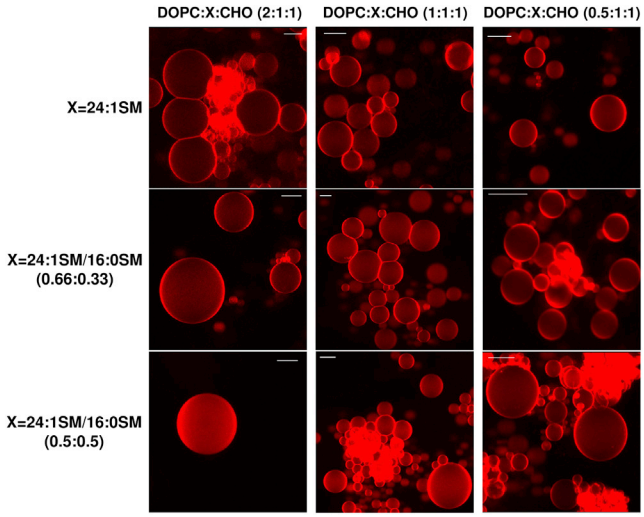

FIGURE 4 Confocal fluorescence microscopy images of Liss-Rho-DOPE-labeled GUVs showing the effect of 24:1 SM on domain formation. The lipid composition of the vesicles was DOPC/SM/CHO (2:1:1, 1:1:1, or 0.5:1:1 molar ratios), where SM was either pure 24:1 SM or mixtures of 24:1 SM and 16:0 SM at ratios of 0.66:0.33 or 0.5:0.5. Scale bar, 10 μm. To see this figure in color, go online.

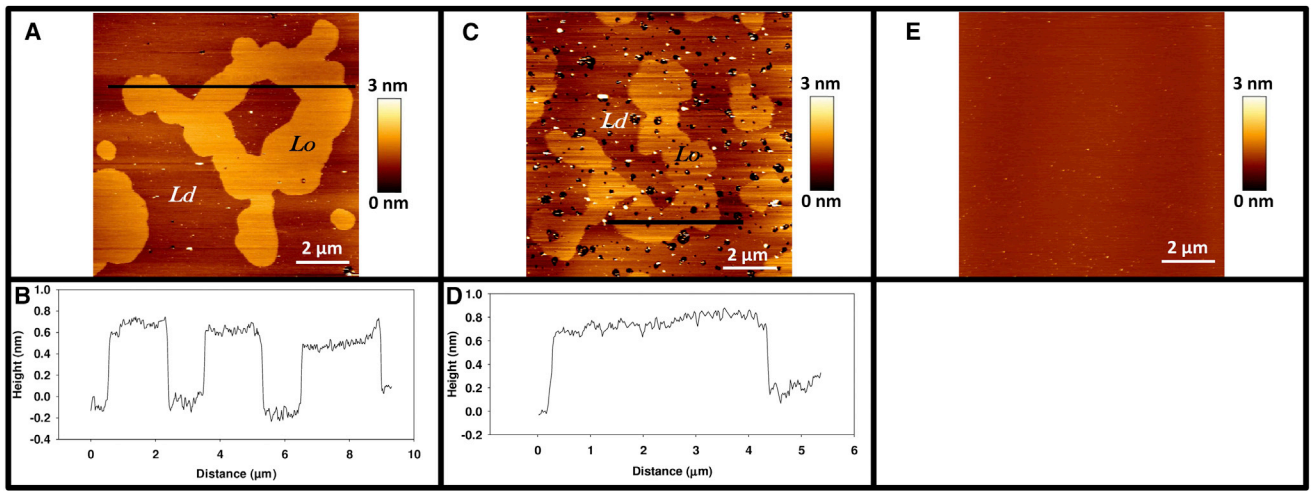

FIGURE 5 AFM images of SPBs. (*A*) AFM topographic image of DOPC/16:0 SM/CHO (2:1:1 molar ratio). (*B*) Height profile measured along the thick black line in *A*. (*C*) AFM topographic image of DOPC/24:0 SM/CHO (2:1:1 molar ratio). (*D*) Height profile measured along the thick black line in *C*. (*E*) AFM topographic image of DOPC/24:1 SM/CHO (2:1:1 molar ratio). To see this figure in color, go online.

found using confocal microscopy, no phase separation was observed in SPBs prepared with 2:1:1 DOPC/24:1 SM/CHO (Fig. 5 *E*).

To further characterize the lipid mixtures topographically described above, we next explored quantitatively the molecular determinants that provide mechanical stability to the different supported membranes. With this aim, AFM force spectroscopy measurements were performed by conducting force curves (Fig. 6) at a constant piezoelectric velocity of 1 μm s^{-1} on the central region of each domain. In addition, breakthrough forces provided measurements of phase-segregated lipid bilayers in the absence of dye label, thus avoiding the occasionally inconsistent partitioning behavior of dye molecules (31).

Fig. 6, *A* and *B*, shows the distribution of breakthrough forces, F_b, in both phases of the SPB made of DOPC/16:0 SM/CHO (2:1:1 molar ratio). From the Gaussian fits to the data, the average rupture force was 5.7 $\pm$ 1.3 nN and 11.3 $\pm$ 2.8 nN for the Ld and Lo phases, respectively. The higher F_b exhibited by the SM/CHO-enriched Lo domains reflects a more efficient packing in the Lo phase than in the DOPC-enriched Ld phase. F_b measured in the mixture DOPC/24:1 SM/CHO (2:1:1, molar ratio) reached an intermediate value of 8.0 $\pm$ 2.1 nN (Fig. 6, *C* and *D*).

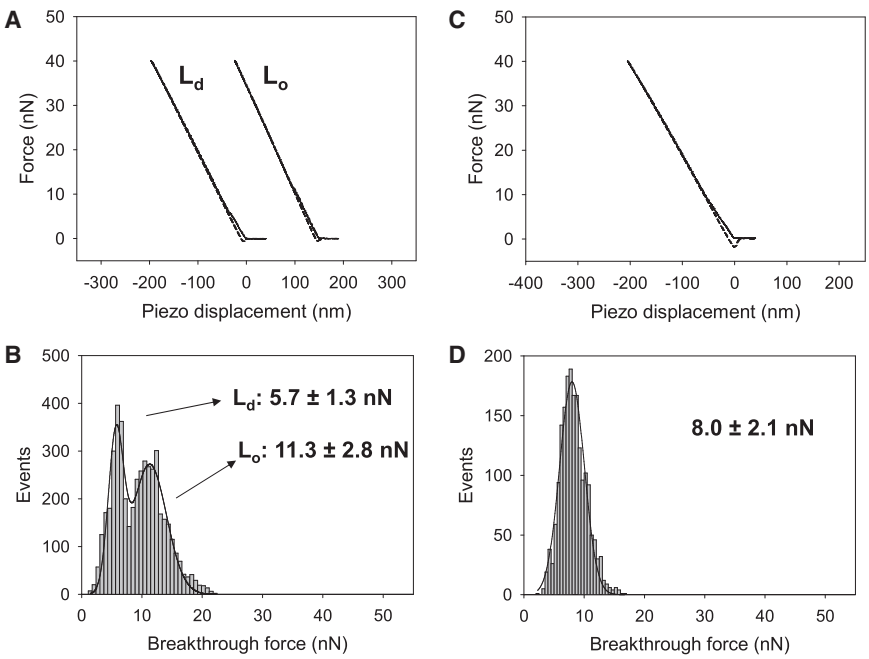

FIGURE 6 AFM force spectroscopy measurements of SPBs. (*A*) Representative force spectroscopy experiment for an SPB made of DOPC/16:0 SM/CHO (2:1:1). (*B*) Distribution of breakthrough forces, F_b, in bilayer shown in Fig. 5 *A*. (*C*) Representative force spectroscopy experiment for an SPB made of DOPC/24:1 SM/CHO (2:1:1). (*D*) Distribution of breakthrough forces, F_b, in bilayer shown in Fig. 5 *E*.

Fig. 7 shows the lateral organization of SPBs (DOPC/16:0 SM/CHO) containing 50, 33, or 20 mol % DOPC. In agreement with the confocal microscopy results, AFM topographic images show that decreasing DOPC produced an increase in the size of Lo domains without impairing lateral segregation (e.g., for the three images shown in Fig. 7, the area covered by the Lo phase was 37%, 52%, and 72%, respectively, for 50, 33, and 20 mol % DOPC). The observation of phase separation in Fig. 7 is in agreement with published phase diagrams of the same lipid mixtures (4), and the percent area/Lo fraction rather closely follows the lever rule (31). Finally, AFM images of DOPC/SM/CHO SPBs containing different amounts of 24:1 SM show the existence of a single phase in all vesicles, for all molar ratios of DOPC/SM/CHO tested (2:1:1; 1:1:1, and 0.5:1:1) (Fig. S2).

Altogether, the results from confocal microscopy and topographic and AFM force spectroscopy measurements show that unsaturation in 24:1 SM has a disordering effect on DOPC/SM/CHO bilayers, with clear consequences for PC/SM/CHO interactions, inducing lipid mixing and consequently preventing phase segregation.

Studies of Laurdan GP in laterally homogeneous lipid bilayers

Laurdan GP reports hydration levels at the lipid-water interface, which in turn are related to the degree of lipid order (32). We measured Laurdan GP in a number of the above studied mixtures for which no lateral heterogeneity was observed by AFM or confocal microscopy. In equimolar phospholipid/CHO mixtures (Fig. 8 *A*), Laurdan shows that 24:1 SM interacting with CHO gives rise to highly ordered bilayers, comparable to those formed by 16:0 SM and CHO. The observation of similar GP values for 16:0 SM/CHO and 24:1 SM/CHO mixtures is interesting and may reflect that the excess length of 24:1 SM relative to 16:0 SM is compensated by the unsaturation to provide a similar degree of molecular order at the interface for these two SM molecules mixed with CHO. The degree of order exhibited under the same conditions by DOPC/CHO bilayers is much lower, as expected from phospholipid unsaturation. Ternary mixtures composed of 24:1 SM, 16:0 SM, and CHO exhibit Laurdan GP values of 0.64 ± 0.002 (0.66:0.33:1) and 0.63 ± 0.003 (0.5:0.5:1), respectively, essentially similar to those measured for 24:1 SM/CHO or 16:0 SM/CHO in Fig. 8 *A*. However, inclusion of DOPC in the 24:1 SM/CHO mixture causes a dose-dependent decrease in Laurdan GP (Fig. 8 *B*). Taken together, the results shown in Figs. 2, 4–6, and 8 suggest that 24:1 SM plays a role in preventing phase segregation while keeping a certain degree of lipid order. Lipid order would be decreased by other lipids, e.g., DOPC.

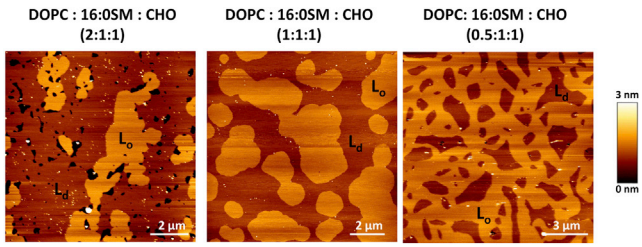

FIGURE 7 AFM images of SPBs. AFM topographic images of SPBs made of DOPC/16:0 SM/CHO at molar ratios of 2:1:1 (*left*), 1:1:1 (*center*), and 0.5:1:1 (*right*) were taken in contact mode in buffer. To see this figure in color, go online.

Studies on erythrocyte membranes

24:1 is a common acyl chain in SM from sheep erythrocytes (3). We have studied the influence of 24:1 SM on the lateral organization of erythrocyte membranes from different animal species. GUVs prepared from right-side-out ghosts (G-ghosts) from erythrocyte membranes were prepared as described in Materials and Methods.

Table 2 shows the molar proportions of the major lipid classes of human, sheep, and rabbit erythrocyte ghosts. Whereas the CHO content is roughly similar among the species, significant differences are observed in the relative amounts of PC and SM. Sheep erythrocytes are known to have a high proportion of SM in their membranes (~42%) (23), followed by rabbit (28%) and human erythrocytes (12%). Human ghosts show the highest amount of PC (17%), followed by rabbit ghosts (12%), whereas sheep ghosts are characterized by the absence of this lipid in their membranes (33). The aggregated molar ratios of PE, PS, and PI were only slightly different among the erythrocytes from the three species.

Table 3 compares the 16:0, 24:0, and 24:1 content of molecular species of SM of human, sheep, and rabbit erythrocyte ghosts. Mass spectrometry analysis allowed the determination of the total number of carbon atoms and double bonds in the fatty acid moiety for lipid classes and the assignment to a bond type (acyl or ether). In all SM species, C18:1 sphingosine was the sphingoid base. The major SM molecular species in human erythrocyte ghosts was 16:0 SM (41%), followed by 24:1 (24%), whereas sheep erythrocytes contained 20% 16:0 SM and 42% 24:1 SM. Rabbit erythrocytes were rather similar to human erythrocytes, except that the latter contain a higher proportion of 24:0 SM (20%).

Fig. 9 shows confocal fluorescence microscopy images of Liss-Rho-DOPE-labeled G-ghosts from the three animal erythrocyte membranes described above. We observed no phase separation in any of the G-ghosts assayed. This is to be expected considering the variety of lipids and proteins involved, although the presence of saturated SM and CHO at high concentrations could also lead to separation of Lo domains.

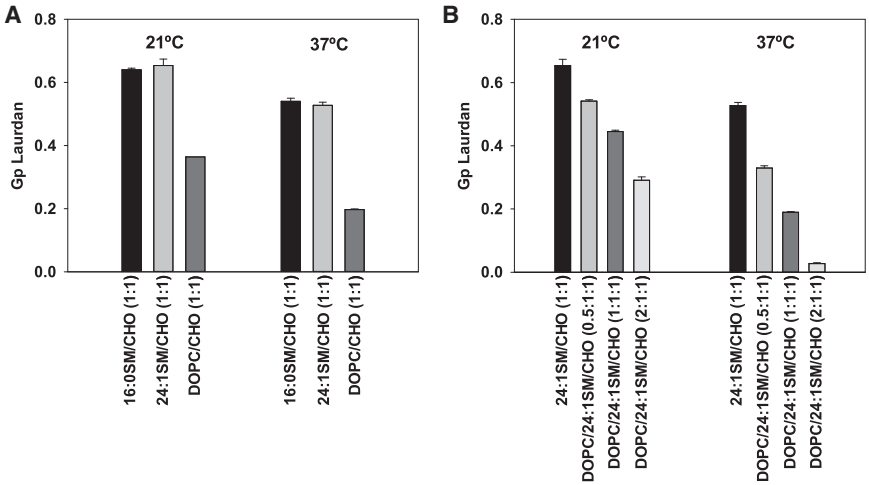

FIGURE 8 Laurdan GP in lipid bilayers at 21°C and 37°C. (*A*) Binary mixtures of 24:1 SM, 16:0 SM, and DOPC with CHO. (*B*) Effects of including DOPC in the 24:1 SM/CHO mixture.

DISCUSSION

Lipid mixtures consisting of PC, SM, and CHO frequently give rise to coexisting Lo (SM/CHO-enriched) and Ld (PC-enriched) domains in bilayers (34). Domains form as a consequence of nonideal mixing of membrane lipid components, which leads to segregation of certain lipids. Despite the fact that 24:1 SM is a common SM in natural membranes, only a few studies have addressed its interaction with other lipids and the consequences for domain formation (4,14,35).

Pure SM and binary SM/CHO bilayers

The presence of the *cis* double bond in the C24 acyl chain of SM leads to just a small decrease in the F_b needed to disrupt SPB (Table 1). As AFM force spectroscopy measurements depend on the molecular interactions between neighboring lipid molecules, it is interesting to correlate F_b values with other biophysical parameters, such as the average area occupied per lipid and the transition temperature from the gel to the liquid-crystalline phase (T_m). In their study using differential scanning calorimetric analysis, Jimenez-Rojo et al. (14) reported transition temperatures for 24:0 SM and 24:1 SM of ~46°C and 24°C, respectively. Thus, the disordering effect of the double bond is clearer for thermal than for mechanical (penetration) properties of the bilayers. Conversely, AFM appears to be more sensitive than the widely used diphenylhexatriene fluorescence polarization in the detection of CHO effects, at least for SM-based mixtures. Whereas our study clearly shows that CHO decreases the F_b in SM bilayers (Table 1), a study by Jaikishan et al. in which CHO content was increased by up to 30 mol % in SM bilayers showed that gel-phase destabilization was not clearly reported by steady-state anisotropy measurements of diphenylhexatriene (36).

TABLE 2 Mol % lipid composition of human, sheep, and rabbit erythrocyte ghosts

Major lipids	Human ghosts[a,b]	Sheep ghosts[b]	Rabbit ghosts[b]
CHO	54.0 ± 3.4	39.2 ± 4.4	45.0 ± 3.5
SM	12.1 ± 2.1	41.5 ± 3.2	27.4 ± 3.7
PC	17.7 ± 1.6	0.0 ± 0.1	12.4 ± 1.7
PE	11.7 ± 0.9	14.0 ± 1.7	13.3 ± 0.7
PI/PS	6.4 ± 0.5	5.1 ± 0.4	2.8 ± 0.3

[a]Koumanov et al (23).
[b]This work.

Effect of 24:1 SM on lateral organization of lipid mixtures

The propensity of 24:1 SM to form lateral domains in mixtures with DOPC and CHO was studied at the meso- and

TABLE 3 Fatty acid composition of amide-linked substituents to sphingomyelin in human, sheep, and rabbit erythrocyte ghosts

Sphingomyelin	Erythrocyte ghosts		
Fatty acid	Human[a]	Sheep[b]	Rabbit[b]
SM15:0	—	1.8	2.8
SM16:0	**41.5**	**19.9**	**34.6**
SM16:1	—	1.0	1.7
SM17:0	—	3.2	2.8
SM18:0	6.2	3.6	4.0
SM18:1	1.1	0.7	1.2
SM18:2	0.1	—	—
SM 20:0	0.7	—	—
SM22:0	5.8	3.6	—
SM22:1	—	1.0	—
SM23:0	—	1.5	3.1
SM24:0	**20.0**	**6.7**	**6.6**
SM24:1	**24.0**	**42.4**	**26.2**
SM24:2	—	9.9	8.4
SM25:1	—	2.4	5.5
SM 26:0	0.4	—	1.4
SM26:1	0.2	2.2	1.8

Bold print indicates the SM molecular species used in this study.
Data are expressed as percent total SM content.
[a]Koumanov et al. (23).
[b]This work.

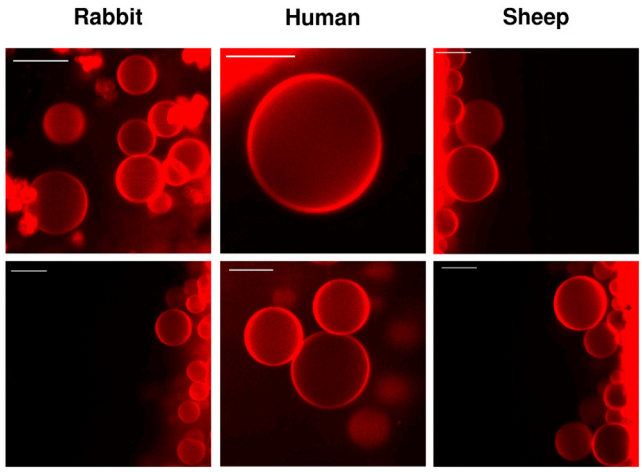

FIGURE 9 Confocal fluorescence microcopy images of Liss-Rho-DOPE-labeled G-ghost. Vesicles from rabbit, human, and sheep erythrocyte membranes (G-ghosts) were prepared as described in Materials and Methods. Scale bar, 10 μm. To see this figure in color, go online.

nanoscale at 20°C by confocal microscopy and AFM, respectively. It is evident from both confocal and AFM images that unlike 16:0 SM and 24:0 SM, 24:1 SM does not induce phase segregation in ternary lipid mixtures with DOPC and CHO, suggesting that 24:1 SM is able to accommodate both DOPC and CHO in a single phase. Interestingly, confocal and AFM images show that at all DOPC/SM/CHO ratios tested, incorporation of 24:1 SM into the membranes, even in the presence of 16:0 SM, prevents domain formation and phase separation (Fig. 4). The same effect has been observed by fluorescence quenching in liposomes of similar composition (POPC/16:0 SM/24:1 SM/CHO, 6:1.5:1.5:1 molar ratio) (35). Thus, the stability of ordered domains was markedly reduced when 24:1 SM was incorporated into the sample, indicating that 24:1 SM mixed with and perturbed the packing of the ordered 16:0 SM and 24:0 SM domains. Moreover, the single F_b value obtained in the SPBs with 24:1 SM, a single-phase system, is intermediate between those of Lo and Ld phases, consistent with the greater miscibility of and specific interaction between 24:1 SM and DOPC. The fact that 24:1 SM prevents formation of Lo phases by saturated SM and CHO may be due to a high miscibility of 24:1 SM with saturated SM. Since 24:1 SM is also miscible with DOPC, the final result is a homogeneous phase.

Our data reinforce the idea expressed by Epand and Epand (37) that the driving force behind creation of larger clusters or domains is not only SM-CHO interactions. The authors showed that although CHO miscibility is greater with oleoyl-SM (C18:1 SM) than with egg-SM (containing >80% 16:0 SM), egg-SM forms domains in fluid membranes containing CHO, whereas oleoyl-SM does not. They suggest that this is a consequence of the greater miscibility of oleoyl-SM with DOPC, so that addition of CHO does not result in the formation of domains with physical properties different from those of the bulk lipid. Conversely, the miscibility of saturated egg SM with DOPC in the DOPC/SM/CHO system is quite low, so that domains do form. Interestingly, Laurdan GP data show that the same degree of molecular order is seen in 24:1 SM/CHO binary mixtures as in C16:0 SM/CHO binary mixtures (Fig. 8). It is only in the presence of DOPC that the overall GP decreases, suggesting a disordering effect, perhaps due to a preferential mixing of 24:1 SM with DOPC over CHO.

The importance of sphingolipid N-acyl chain length in the interaction between glycerophospholipids and CHO for the formation of lateral domains in membranes was recently reviewed by Quinn (38). That model postulated that domains are formed between symmetric molecular species of sphingolipids (with N-acyl fatty acid substituents 16–18C in length) and CHO. These symmetric sphingolipids would interact via intermolecular hydrogen bonds that would prevent them from mixing with glycerophospholipids even at temperatures above the main transition temperature of the lipids, when they are both in the Ld phase. The behavior of asymmetric sphingolipids (N-acyl fatty acids 22–26C in length) in mixtures with glycerophospholipids and CHO would be different. Based on pulsed-field-gradient NMR spectroscopy measurements (39), it was reported that asymmetric sphingolipids mix with phospholipids to form stoichiometric complexes and do not give rise to coexisting bilayer phases in ternary mixtures with CHO and PC. Björkqvist et al. reported that CHO in mixtures with C24:0 SM, either alone or together with C16:0 SM, form stable ordered domains in fluid bilayers of glycerophospholipids with CHO (35). However, 24:0 SM segregates with CHO to form Lo domains (Fig. 2), whereas 24:1 SM does not, supporting the notion that both unsaturation and SM N-acyl chain length determine the interactions between the three lipids.

Biological membranes

In establishing a set of principles of lipid phase behavior in molecular systems, the potential importance of minor lipid species in the structure of cell membrane domains has been more or less ignored. In fact, biological membranes are composed of a plethora of lipid molecular species. In this context, it has been suggested by some authors that Lo domains enriched in SM and CHO are present in biological membranes, and particularly in erythrocyte membranes, based on the resistance of those membrane domains to solubilization at 4°C by nonionic detergents such as Triton X-100 (23,40). However, confocal images of Liss-Rho-DOPE-labeled G-ghosts from human, sheep, and rabbit erythrocyte membranes (Fig. 9) show no phase separation. In all cases, the presence of SM and CHO could in principle lead to the formation of Lo domains in the erythrocytes under study, although in practice such domains cannot be observed. When the different SM molecular species are considered, both saturated and unsaturated species are found

at molar ratios of 3:1 (humans), 0.66:1 (sheep), and 1:1 (rabbit). The most abundant species in all three cases are 16:0 (saturated) and 24:1 (unsaturated). This suggests that 24:1 SM may play a crucial role in preventing lateral phase separation in red blood cell membranes. Moreover, these results point once again to the misleading conclusions that can be drawn from detergent-extraction experiments, reflecting limitations of the Triton X-100 assay as applied to natural and/or synthetic membranes (9). The reason why cell plasma membrane lipids do not separate into macroscopic domains has remained at issue since the raft hypothesis was first proposed (6). There are many possible explanations, e.g., intracellular membrane traffic, but our data concerning one significant lipid component in plasma membranes may also contribute to the interpretation of the biological data.

Finally, little is known about the functional importance of 24:1 SM in certain animal tissues and cells, such as bovine brain (42), HL-60 cells (43), or sheep erythrocytes (3), that have evolved to contain high levels of this long and unsaturated molecule in their membranes. It has been reported that 24:1 SM levels are linked to central nervous system developmental processes such as myelin maturation (44). *Clostridium perfringens* alpha toxin induces hemolysis of sheep erythrocytes by activating the metabolism of 24:1 SM via a GTP-binding protein in membranes (40). In sheep erythrocytes, it is also possible that 24:1 SM is needed to confer increased fluidity to the membranes, which lack PC. Moreover, the long and unsaturated nature of the 24:1 SM molecule may have a substantial effect on its interactions with membrane proteins. This interesting lipid provides a further example to understand the need for complexity in the structures of natural sphingolipids (14).

CONCLUSION

The main emphasis to date in assigning the role of lipids in membrane domain formation has been on the creation of Lo phases mediated by interaction of CHO with sphingolipids, principally SM. In this study, the influence of 24:1 SM on the lateral organization and nanomechanical stability of model and natural membranes has been examined. The main conclusion is that 24:1 SM is unable to form Lo domains in the presence of DOPC and CHO, and that this is due, at least in part, to the N-acyl chain unsaturation. In general, CHO does not appear to interact equally with different SMs. The particular properties conferred on sphingolipids by unsaturation have implications for the formation of lipid domains in cell membranes. Unsaturated SMs can be seen as one of Nature's tools for preventing lateral phase separation in cell membranes.

SUPPORTING MATERIAL

Two figures are available at http://www.biophysj.org/biophysj/supplemental/S0006-3495(14)00509-8.

L.B. and S.M. are members of the Carrera del Investigador Comisión de Investigaciones Científicas de la Provincia de Buenos Aires (CICBA), Argentina. V.H. is a member of the Carrera del Investigador of CONICET. R.V. is a fellow of the Consejo Nacional de Investigaciones Científicas y Técnicas (CONICET), Argentina. The authors are grateful to Dr. Donald F. Haggerty, a retired career investigator and native English speaker, for editing the final version of the manuscript.

This work was supported by grants from the Comisión de Investigaciones Cientificas de la Provincia de Buenos Aires and the Agencia Nacional de Promoción Científica PICT (no. 2129), from the Spanish Ministry of Economy (BFU 2012-36241), and from the Basque Government (IT838 and IT849-13).

REFERENCES

1. Barenholz, Y., and T. E. Thompson. 1980. Sphingomyelins in bilayers and biological membranes. *Biochim. Biophys. Acta.* 604:129–158.
2. Jaikishan, S., and J. P. Slotte. 2011. Effect of hydrophobic mismatch and interdigitation on sterol/sphingomyelin interaction in ternary bilayer membranes. *Biochim. Biophys. Acta.* 1808:1940–1945.
3. Peter Slotte, J. 2013. Molecular properties of various structurally defined sphingomyelins—correlation of structure with function. *Prog. Lipid Res.* 52:206–219.
4. Nyholm, T. K. M., D. Lindroos, …, J. P. Slotte. 2011. Construction of a DOPC/PSM/cholesterol phase diagram based on the fluorescence properties of *trans*-parinaric acid. *Langmuir.* 27:8339–8350.
5. Lönnfors, M., J. P. Doux, …, J. P. Slotte. 2011. Sterols have higher affinity for sphingomyelin than for phosphatidylcholine bilayers even at equal acyl-chain order. *Biophys. J.* 100:2633–2641.
6. Simons, K., and E. Ikonen. 1997. Functional rafts in cell membranes. *Nature.* 387:569–572.
7. Quinn, P. J., and C. Wolf. 2009. Thermotropic and structural evaluation of the interaction of natural sphingomyelins with cholesterol. *Biochim. Biophys. Acta.* 1788:1877–1889.
8. Giocondi, M. C., D. Yamamoto, …, C. Le Grimellec. 2010. Surface topography of membrane domains. *Biochim. Biophys. Acta.* 1798:703–718.
9. Lichtenberg, D., F. M. Goñi, and H. Heerklotz. 2005. Detergent-resistant membranes should not be identified with membrane rafts. *Trends Biochem. Sci.* 30:430–436.
10. Térová, B., R. Heczko, and J. P. Slotte. 2005. On the importance of the phosphocholine methyl groups for sphingomyelin/cholesterol interactions in membranes: a study with ceramide phosphoethanolamine. *Biophys. J.* 88:2661–2669.
11. Kuikka, M., B. Ramstedt, …, J. P. Slotte. 2001. Membrane properties of D-erythro-N-acyl sphingomyelins and their corresponding dihydro species. *Biophys. J.* 80:2327–2337.
12. Nyholm, T. K., M. Nylund, and J. P. Slotte. 2003. A calorimetric study of binary mixtures of dihydrosphingomyelin and sterols, sphingomyelin, or phosphatidylcholine. *Biophys. J.* 84:3138–3146.
13. Ramstedt, B., and J. P. Slotte. 1999. Comparison of the biophysical properties of racemic and d-erythro-N-acyl sphingomyelins. *Biophys. J.* 77:1498–1506.
14. Jiménez-Rojo, N., A. B. García-Arribas, …, F. M. Goñi. 2014. Lipid bilayers containing sphingomyelins and ceramides of varying N-acyl lengths: a glimpse into sphingolipid complexity. *Biochim. Biophys. Acta.* 1838 (1 Pt B):456–464.
15. Montes, L. R., H. Ahyayauch, …, F. M. Goñi. 2010. Electroformation of giant unilamellar vesicles from native membranes and organic lipid mixtures for the study of lipid domains under physiological ionic-strength conditions. *Methods Mol. Biol.* 606:105–114.
16. Angelova, M. I., and D. S. Dimitrov. 1986. Liposome electroformation. *Faraday Discuss. Chem. Soc.* 81:303–311.

17. Dimitrov, D. S., and M. I. Angelova. 1988. Lipid swelling and liposome formation mediated by electric fields. *Bioelectrochem. Bioenerg.* 19:323–336.

18. Jass, J., T. Tjärnhage, and G. Puu. 2000. From liposomes to supported, planar bilayer structures on hydrophilic and hydrophobic surfaces: an atomic force microscopy study. *Biophys. J.* 79:3153–3163.

19. Garcia-Manyes, S., L. Redondo-Morata, …, F. Sanz. 2010. Nanomechanics of lipid bilayers: heads or tails? *J. Am. Chem. Soc.* 132:12874–12886.

20. Chen, P., T. Toribara, and H. Warner. 1956. Microdetermination of phosphorus. *Anal. Chem.* 28:1756–1758.

21. Bligh, E. G., and W. J. Dyer. 1959. A rapid method of total lipid extraction and purification. *Can. J. Biochem. Physiol.* 37:911–917.

22. Quinn, P. J., D. Rainteau, and C. Wolf. 2009. Lipidomics of the red cell in diagnosis of human disorders. *Methods Mol. Biol.* 579:127–159.

23. Koumanov, K. S., C. Tessier, …, P. J. Quinn. 2005. Comparative lipid analysis and structure of detergent-resistant membrane raft fractions isolated from human and ruminant erythrocytes. *Arch. Biochem. Biophys.* 434:150–158.

24. Butt, H.-J. 1991. Measuring electrostatic, van der Waals, and hydration forces in electrolyte solutions with an atomic force microscope. *Biophys. J.* 60:1438–1444.

25. Müller, D. J., and A. Engel. 1997. The height of biomolecules measured with the atomic force microscope depends on electrostatic interactions. *Biophys. J.* 73:1633–1644.

26. Picas, L., C. Suárez-Germà, …, J. Hernández-Borrell. 2010. Force spectroscopy study of Langmuir-Blodgett asymmetric bilayers of phosphatidylethanolamine and phosphatidylglycerol. *J. Phys. Chem. B.* 114:3543–3549.

27. de Almeida, R. F., L. M. Loura, …, M. Prieto. 2005. Lipid rafts have different sizes depending on membrane composition: a time-resolved fluorescence resonance energy transfer study. *J. Mol. Biol.* 346:1109–1120.

28. Juhasz, J., J. H. Davis, and F. J. Sharom. 2010. Fluorescent probe partitioning in giant unilamellar vesicles of "lipid raft" mixtures. *Biochem. J.* 430:415–423.

29. Baumgart, T., G. Hunt, …, G. W. Feigenson. 2007. Fluorescence probe partitioning between Lo/Ld phases in lipid membranes. *Biochim. Biophys. Acta.* 1768:2182–2194.

30. Connell, S. D., and D. A. Smith. 2006. The atomic force microscope as a tool for studying phase separation in lipid membranes. *Mol. Membr. Biol.* 23:17–28.

31. Sullan, R. M., J. K. Li, …, S. Zou. 2010. Cholesterol-dependent nanomechanical stability of phase-segregated multicomponent lipid bilayers. *Biophys. J.* 99:507–516.

32. Dietrich, C., L. A. Bagatolli, …, E. Gratton. 2001. Lipid rafts reconstituted in model membranes. *Biophys. J.* 80:1417–1428.

33. Christie, W. W. 1981. Lipid Metabolism in Ruminant Animals. Pergamon, Oxford, pp. 95–191.

34. Goñi, F. M., A. Alonso, …, J. L. Thewalt. 2008. Phase diagrams of lipid mixtures relevant to the study of membrane rafts. *Biochim. Biophys. Acta.* 1781:665–684.

35. Björkqvist, Y. J., J. Brewer, …, B. Westerlund. 2009. Thermotropic behavior and lateral distribution of very long chain sphingolipids. *Biochim. Biophys. Acta.* 1788:1310–1320.

36. Jaikishan, S., A. Björkbom, and J. P. Slotte. 2010. Sphingomyelin analogs with branched N-acyl chains: the position of branching dramatically affects acyl chain order and sterol interactions in bilayer membranes. *Biochim. Biophys. Acta.* 1798:1987–1994.

37. Epand, R. M., and R. F. Epand. 2004. Non-raft forming sphingomyelin-cholesterol mixtures. *Chem. Phys. Lipids.* 132:37–46.

38. Quinn, P. J. 2010. A lipid matrix model of membrane raft structure. *Prog. Lipid Res.* 49:390–406.

39. Filippov, A., G. Orädd, and G. Lindblom. 2006. Sphingomyelin structure influences the lateral diffusion and raft formation in lipid bilayers. *Biophys. J.* 90:2086–2092.

40. Oda, M., T. Matsuno, …, J. Sakurai. 2008. The relationship between the metabolism of sphingomyelin species and the hemolysis of sheep erythrocytes induced by *Clostridium perfringens* alpha-toxin. *J. Lipid Res.* 49:1039–1047.

41. Reference deleted in proof.

42. Boegheim, Jr., J. P. J., M. Van Linde, …, B. Roelofsen. 1983. The sphingomyelin pools in the outer and inner layer of the human erythrocyte membrane are composed of different molecular species. *Biochim. Biophys. Acta.* 735:438–442.

43. Fitzgerald, V., M. L. Blank, and F. Snyder. 1995. Molecular species of sphingomyelin in sphingomyelinase-sensitive and sphingomyelinase-resistant pools of HL-60 cells. *Lipids.* 30:805–809.

44. Babin, F., P. Sarda, …, A. Crastes de Paulet. 1993. Nervonic acid in red blood cell sphingomyelin in premature infants: an index of myelin maturation? *Lipids.* 28:627–630.